Experimental and analytical study to evaluate the effectiveness of an in-plane reinforcement for masonry walls using GFRP meshes

Natalino Gattesco [1], Ingrid Boem *

Department of Engineering and Architecture, University of Trieste, Piazzale Europa 1, 34127 Trieste, Italy

HIGHLIGHTS

- Diagonal compression test on masonry strengthened with GFRP reinforced mortar coating.
- Influence of type of masonry and of the mortar for the coating investigated.
- Great improvements in resistance and dissipative capacity of reinforced walls.
- Analytical formulation for the evaluation of the tensile strength of reinforced walls.

ARTICLE INFO

Accepted 12 April 2015

Keywords:
Seismic retrofitting
Structural rehabilitation
Masonry structures
Strengthening technique
Experimental test
Composite material
GFRP mesh

ABSTRACT

The paper collects the results of diagonal compression tests to compare the in-plane behavior of unreinforced masonry (URM) and of masonry strengthen with a GFRP reinforced mortar coating. Experimental tests concern square wallettes of different masonry types and thickness; different mortars are considered for the coating. Significant increasing both in resistance and ductility emerges in reinforced masonry (RM). The principal tensile strengths are derived from experimental results and an analytical formulation is proposed for the RM resistance prediction. The formulation evidences that the contribution of the reinforced mortar coating is influenced by the characteristics of both the masonry and the reinforcement.

1. Introduction

The architectural heritage of European cities consists mostly of buildings made with unreinforced masonry (URM) walls and wooden floors. The very low tensile and flexural resistances of existing masonry and its brittle behavior are responsible of the high seismic vulnerability of these buildings, as evidenced also in the recent earthquakes in East Slovenia 1998–2004, Southern Greece 2006–2008, Central Italy 2009, Northern Italy 2012, and thus strengthening interventions are needed to increase both in-plane and out-of-plane resistance of masonry walls.

Normally, the out-of-plane action may be considerably reduced connecting effectively the walls to floors with adequate in-plane stiffness [1,2], avoiding in this way the local collapse of masonry elements (wall overturning, vertical and/or horizontal bending, overturning of the building corner, collapse of the gable, etc.). The shear rupture of masonry piers and spandrel beams, which leads to the global collapse of the building, was prevented in the past by traditional techniques such as grout injections [3–5], application of steel-reinforced concrete overlays [6–8] or repointing mortar joints [9,10]. The grouting injection technique, extensively used to strengthen multiple leaf masonry, is not adequate for many types of walls (e.g. single leaf walls, cobblestone masonry, rubble stone masonry, etc.) and the use of steel elements in reinforced plaster evidenced, in the long term, severe problems of corrosion of the reinforcement.

For this reason, in the last two decades, several strengthening techniques based on the use of non-metallic elements such as polymeric materials were proposed [11–13] because of their low sensitivity to environmental agents, making the reinforcing system more suitable for applications even under severe operating conditions. The composite materials employed in seismic enhancement of masonry construction are, mostly, FRP (fiber reinforced polymers) based on carbon, glass or aramid fiber but also the use of

* Corresponding author.
E-mail addresses: gattesco@units.it (N. Gattesco), boem@dicar.units.it (I. Boem).
[1] Tel.: +39 040 5583840; fax: +39 040 5583580.

PP (polypropylene) or PBO (poliparafenilenbenzobisoxazole) polymeric elements has been investigated. Depending on the type of composite and on the element used (fabrics, strips, bars or meshes), the reinforcements are utilized in the mortar joint as reinforced repointing, are glued directly to the masonry through either epoxy resin or a thin mortar plaster or are embedded in a mortar coating.

The repointing of mortar joints with FRP bars [14,15] or strips [16–18] performed good results in terms of in-plane strength and deformation capacity of URM for single leaf regular masonry; moreover, the technique limits additional masses in the building and permits the conservation of the aspect of fair-face walls. But, this reinforcing technique has limited effectiveness for out-of-plane actions because the resistance increase for vertical bending is negligible. Moreover, the technique is suitable only for regular masonry and it is not effective for multiple leaf masonry, because no transversal connections are planned. Also externally bonded laminates [19–22] or meshes [23–28] affect limitedly the masonry weight and show important improvements in the in-plane shear resistance and deformation capacity. This reinforcement system, as the repointing technique, is suitable only for single leaf masonry, in the other cases some transversal connectors (diatones) need to be added. To glue effectively the strips it is necessary to regularize the surface with appropriate high bond mortar, nevertheless its effectiveness is limited by debonding failure.

The application of FRP meshes embedded in a mortar coating [29–33] on both wall faces permits to increase in-plane shear and out-of-plane bending resistance raising significantly also the plastic deformation capacity. To avoid the separation of wall leafs and to make effective the reinforcement some passing-through connectors are applied. The presence of a thicker coating increases the additional mass but allows the use of natural binders for the coating, as lime and pozzolan, instead of cement, making the reinforcement compatible with the masonry components and permitting its application also on listed architectural assets. In case of fair-face walls this technique may be modified by coupling the FRP reinforced mortar coating on one face of the wall with a reinforced repointing on the other one [34]. Moreover, the proposed strengthening technique could also be useful for retrofitting infill frame existing structures to resist horizontal loads by improving, with such a surface intervention, the in-plane behavior of the infill walls and consequently providing better performances to the whole structure [35].

The present study investigates the mechanical behavior of masonry walls strengthen with a GFRP mesh reinforced mortar coating, which is effective in seismic enhancement of URM buildings both for in-plane [33] and out-of-plane actions [36]. In [33] were presented and discussed the results of a wide number of diagonal compression tests carried out on solid brick masonry (250 mm and 380 mm thick), two-leaf solid brick masonry with rubble conglomerate infill and rubble stone masonry. The tensile strength, the shear modulus and the ductility of URM and RM were investigated, considering different mortars for the masonry and different reinforcement percentages. The results proved the great effectiveness of the technique and evidenced that the lower is the tensile strength or the stiffness of unreinforced samples, the higher is the increase in reinforced samples. No appreciable differences emerged in tensile strength and shear modulus of specimens reinforced with different percentages of reinforcement, because the tensile strength and the stiffness of the reinforced coating is negligibly influenced by the composite before cracking. Whereas the GFRP mesh has great importance in the post-peak behavior of the RM, providing tensile resistance after cracking through the stress redistribution and permitting the masonry to reach significant values of the deformation capacity (ductility).

In this paper, different types of masonry were tested (solid brick masonry 250 mm thick, cobblestone masonry, rubble stone masonry 400 mm and 700 mm thick) and the influence of different types of mortar for the coating is evaluated. The aim of the paper is to present and discuss the results of the experimental campaign, illustrating the failure mechanism of the different specimens, comparing the behavior of URM and RM specimens and evidencing the effectiveness of the reinforcement. Moreover, it is presented a general analytical formulation useful to assess the resistance increase due to the proposed strengthening method, as no specific recommendations in the building codes (e.g. EC8 [37], FEMA [38–40]) or in the technical literature are nowadays available for the quantification of resistance and ductility increments for such a technique. Current design guidelines (e.g. CNR-DT 203/2006 [41]) refers to structures reinforced with epoxy-bonded FRP laminates and are not suitable for such a technique, as the mortar coating does not act simply as a bonding layer but significantly influence the resistance and displacement capacity of the RM (as evidenced in the paper). The dimensioning criteria of the GFRP-mesh reinforced mortar coating cannot be compared with the application of steel-reinforced concrete wall overlays, because in that technique the whole demand is entrusted to the reinforced coating, due to the relatively high strength and stiffness of the concrete compared to the masonry.

2. Materials and methods

The experimental campaign concerns diagonal compression tests carried out on masonry wallettes, made with different types of units (solid bricks, cobblestones and rubble stones) and to various types of mortar coating used to strengthen the masonry. The geometrical and material characteristics of the specimens used for the tests are detailed in the follow.

2.1. Specimens

A total of 27 square masonry specimens ($1160 \times 1160\ mm^2$ – Fig. 1a) were tested: 6 solid brick samples 250 mm thick, 8 cobblestone samples 400 mm thick, 7 rubble stone samples 400 mm thick and 6 rubble stone samples 700 mm thick. In solid brick masonry specimens, the bricks were all arranged as headers (diatones).

The strengthening technique (Fig. 1b) consists in the application, on both faces of the masonry, of a thin layer of scratch, the execution of some passing through holes, 25 mm diameter, the application of a GFRP mesh, the insertion of L-shaped GFRP connectors ($8 \times 12\ mm^2$), from both sides, into the holes and injected with thixotropic epoxy resin and finally the application of a mortar coating (30–40 mm thick). The connectors are lap spliced inside the wall for a minimum of 200 mm, to guarantee an adequate resistance against connector pull-out [33]. RM specimens were strengthened using 5 GFRP connectors. The actual thickness of the mortar coating was 30 mm for solid brick masonry; in cobblestone and rubble stone specimens, due to irregularities of the masonry surface, the thickness varies from 30 to 45 mm.

2.2. Masonry characteristics

As stated, three different types of masonry were considered in the study: solid bricks, cobblestones and rubble stones. The average resistance of solid bricks subjected to compression tests was $f_b = 44.0$ MPa. Stone elements were all sandstones. For rubble stones masonry, the unit dimensions were roughly $130 \times 230 \times 200\ mm^3$ (respectively height, width and depth); cobblestones specimens had elements with average dimensions $90 \times 90 \times 130\ mm^3$. The mortar joints were 10 mm thick in solid brick specimens; in stone masonry the units were arranged as close as possible so to limit the mortar joint dimensions.

Four types of hydraulic lime mortar were used for masonry specimens: type A, D, E and F. Table 1 resumes the compressive strengths, obtained from cylindrical samples tested at about 60 days air curing. Cylinders had 100 mm diameter and 200 mm height. It is observed that the mortar of some samples evidenced resistances different to those of other samples made with the same dosage. As specimens were made on different days, these differences are attributable to small dissimilarities in the particle size distribution of the sand and mainly to slightly diverse environmental conditions during the setting/curing of the mortar. For this reason, type D and type E mortar are kept separate, even though they have the same binder dosage.

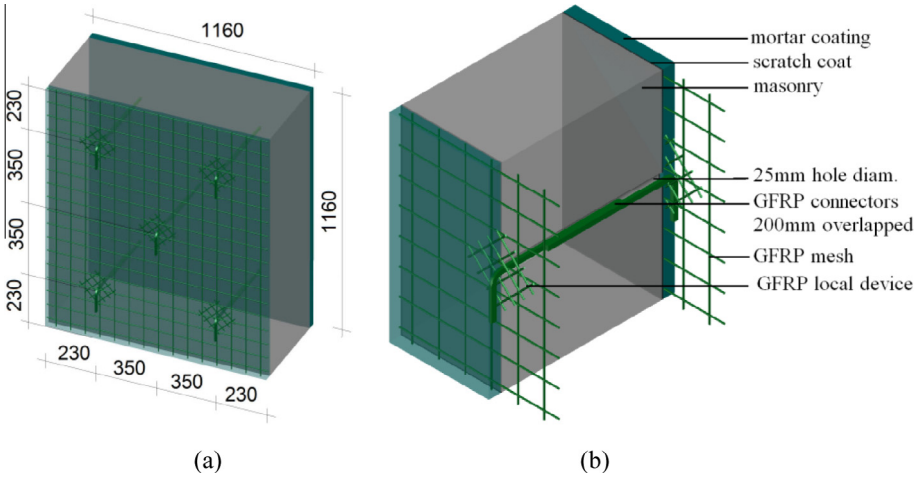

Fig. 1. Main geometrical characteristics of specimens (a) and application procedure of reinforcing (b).

Table 1
Masonry lime mortars: binder dosage (kg of hydraulic lime per m^3 of mortar), cylinder compressive strength ($f_{c,b}$) and coefficient of variation of $f_{c,b}$ (c.o.v.).

Mortar ID	Binder dosage [kg/m^3]	$f_{c,b}$ [MPa]	c.o.v. ($f_{c,b}$) [%]
A	320	2.93	9.9
D	350	4.09	4.9
E	350	3.52	6.5
F	200	1.30	10.0

2.3. Reinforcement characteristics

Different types of mortar were used for the mortar coating: two types of natural hydraulic lime mortar (L and N), one mixed cement-lime mortar (M) and one natural hydraulic lime and pozzolan mortar (Z). In Table 2 are reported the dosages and the mechanical properties of mortars, evaluated on cylindrical samples by compression and indirect tensile tests, both carried out after about 60 days air curing. The cylinders dimensions were: 100 mm diameter and 200 mm or 100 mm height. The compressive strength obtained from cylinders 100 mm tall (mortar type L) was modified in accordance to FEMA 274 [38] so to obtain the cylinder compressive strength $f_{c,c}$ to be compared with that obtained from the samples 200 mm tall.

The GFRP reinforcement utilized in the coating has a mesh 66 × 66 mm^2 and wires with 3.8 mm^2 (type S) and 7.6 mm^2 (type D) fiber cross area. The L-shaped connectors passing through the masonry have a cross section 8 × 12 mm^2 and a fiber cross area equal to 57.6 mm^2. The mechanical characteristics of mesh wires and connectors were determined through tension tests, in accordance to CNR DT 203/2006 – Appendix B [41]. In particular the tensile resistance (T), the ultimate elongation (ε_{ult}) and the axial stiffness (EA) of the specimens tested are summarized in Table 3. Some pull-out tests were carried out in [33] to prove the effectiveness of 200 mm lap splice of connectors inside the holes of the masonry and several bond tests were carried out on Type "S" GFRP mesh embedded in the mortar coating with 130 mm anchorage length [42]. Both tests evidenced good effectiveness.

3. Experimental tests and results

The main characteristics of the test setup and the results of the diagonal compression tests are reported in the section.

3.1. Specimens characteristics

The diagonal compression tests were performed on the masonry specimens indicated in Table 4. Each specimen was identified with an alphanumeric string split in three parts: the first distinguishes the masonry material (B2 = solid brick, C = cobblestone masonry, R4 = 400 mm thick rubble stone and R7 = 700 mm thick rubble stone) and the type of mortar for the masonry (A, D, E and F – Table 1), the second identifies the type of mortar for the coating (L, N, M and Z – Table 2) and the last differentiates equal specimens, because two specimens were normally performed for each configuration so to check the repeatability of the results. URM specimens, obviously, do not have the intermediate part of the string. In all RM specimens a Type "S" GFRP mesh was used with the exception of specimens R7E-M-2 and R7E-Z-2, in which a "Type D" GFRP mesh was utilized. In a previous study [33], in fact, emerged that an higher GFRP reinforcement content influences very little the maximum resistance but the resistance decrease after the peak was less pronounced; therefore, in thick walls such as those of type R7, one reinforced specimen was arranged with standard GRFP grid and the other with a doubled reinforcement content. In the paper are also reported the results of two diagonal compression tests carried out in a previous experimental campaign [33] on solid brick URM specimens (B2A-1 and B2A-2), that were used to compare the behavior of URM and RM specimens.

3.2. Experimental apparatus and test procedure

Two welded stiffened steel angles (steel devices 1, 2) were applied at opposite corners of the specimen and a third device, arranged at the top corner, was connected to the bottom device through two couples of steel bars (Fig. 2). A hydraulic jack (950 kN), interposed between the top devices and activated with a hand pump (700 bar), provided the diagonal force, measured with a pressure transducer. On both faces of the specimen, a couple of potentiometer transducers (T1 and T3, T2 and T4) monitored the diagonals deformations on a measure base of 1100 mm. All transducers were connected to an electronic acquisition unit interfaced with a computer, which permitted to control the progress of the test.

A sequence of loading-unloading cycles with steps of 25–50 kN was performed up to reaching the peak load, then the test was controlled at displacement steps. The load and diagonals deformations were registered on the computer and displayed in graphic form during the test.

3.3. Results

The curves representing the diagonal load P in function of the average diagonal compressive and tensile strains (ε_c and ε_t) and are illustrated in Fig. 3. In the figures, the curves were cut at a value of the compressive and tensile strains equal to |0.005|. This value is approximately 10–15 times greater than the compressive deformation at the end of the elastic limit of strengthened samples. For

Table 2
Binder dosage and mechanical characterization of mortar coating: cylinder compressive strength ($f_{c,c}$), Young modulus (E_c) and tensile strength $f_{t,c}$, with corresponding coefficients of variation (c.o.v.).

Mortar ID	Binder dosage	$f_{c,c}$ [MPa]	c.o.v. ($f_{c,c}$) [%]	E_c [MPa]	c.o.v. (E_c) [%]	$f_{t,c}$ [MPa]	c.o.v. ($f_{t,c}$) [%]
L	300 kg lime per m^3 of mortar	3.64 (4.23[a])	4.5	14,475	3.3	0.55	10.9
N	Pre-mixed compound (Röfix 954)	4.66	13.0	13,796	11.8	0.77	5.2
M	300 kg lime, 100 kg cement per m^3 of mortar	7.35	11.1	14,429	14.2	1.05	7.6
Z	Pre-mixed compound (Grigolin – Palladio)	11.66	12.4	13,431	13.8	1.44	9.0

[a] Compressive strength obtained by tests on cylinders 100 mm tall.

Table 3
Mechanical characteristics of GFRP elements: tensile resistance (T), ultimate elongation (ε_{ult}) and axial stiffness (EA) of one wire, with respective coefficients of variation (c.o.v.).

GFRP element	T [kN]	c.o.v. (T) [%]	ε_{ult} –	c.o.v. (ε_{ult}) [%]	EA [kN]
Type "S" (fiber area 3.8 mm^2)					
Parallel fiber wires	5.62	4.8	0.0193	5.7	291
Twisted fiber wires	4.49	6.7	0.0169	9.5	266
Type "D" (fiber area 7.6 mm^2)					
Parallel fiber wires	8.49	5.5	0.0158	10.8	539
Twisted fiber wires	5.21	3.6	0.0094	22.3	556
Connectors (fiber area 57.6 mm^2)	36.01	2.9	–	–	–

graphic readability, the envelope curves are shown, omitting the branches of unloading and reloading of the various cycles. The load-deformation curves concerning the specimen B2A-Z-1 is omitted, because a construction defect emerged during the test that caused a premature failure.

URM specimens evidenced the formation of a diagonal crack along the force direction as illustrated in Fig. 4. In solid brick masonries (Fig. 4a), the path of the crack follows head and bed mortar joints and it spreads rapidly, resulting in an abrupt decrease of masonry resistance. On the contrary, in cobblestone specimens (Fig. 4b), the crack is approximately linear and the decrease of resistance after the crack formation is considerably attenuated by an important interlocking effect due to the geometry of stone units, which interact one another, resulting in a significant contrast to the crack opening. Rubble stone masonry (Fig. 4c) manifested an intermediate behavior: the cracking follows mainly the mortar joints but, due to the irregular shape of the units, a significant resistance to crack opening occurred, in fact the curves shows a slight resistance decrease after the occurrence of cracking.

In RM specimens a linear diagonal crack formed in the mortar coating, in the force direction, just before reaching the maximum diagonal force (Fig. 5a); gradually the cracking zone spreads with the formation of other cracks, almost parallel to the first one (Fig. 5b), up to the failure of the mesh wires (Fig. 5c). Instead, the cracking of the masonry showed the same trend evidenced in URM specimens. The GFRP mesh intervened in the cracked areas of mortar coating: the reinforcement contrasts the opening of cracks supporting tensile stresses, resulting in a gradual and moderate decrease of the RM resistance in the post-peak branch. The collapse of GFRP wires did not occur up to significant values of the deformation (0.8–1.0%). No evident out-of-plane swellings in the masonry or slips between the masonry and the mortar coating occurred for compressive strains ε_c minor than 0.8–0.9%. These results seems to indicate that in diagonal compression tests the number of connections between reinforcement and masonry does not affect appreciably the shear strength of reinforced specimens. However, it is important to evidence that the connectors play an important role in the confining of masonry subjected to the combined action of shear and compression forces, as evidenced in [43].

The curves P–ε_c of diagonal compression tests permit to identify, for each specimen, the maximum diagonal compressive load (P_{max}); the ratio between the maximum load of RM specimen and the average maximum load of the URM ones ($P_{max(R)}/P_{max(U)}$) evidences the resistance increase due to the strengthening technique. These values are summarized in Table 5. In the table are also reported the yield deformation γ_y of the equivalent elastic-plastic system with secant stiffness at 70% of the maximum load (Fig. 6) [44], the post-peak shear strain $\gamma_{0.8} = \varepsilon_{t,0.8} - \varepsilon_{c,0.8}$, when the load capacity has undergone a 20% reduction (considered as the maximum wall drift), and the ratio $\mu = \gamma_{0.8}/\gamma_y$. This value evidences

Table 4
Specimens characteristics.

Specimen	Masonry mortar	Mortar coating	GFRP mesh type	Specimen	Masonry mortar	Mortar coating	GFRP mesh type
Solid brick masonry, 250 mm thick				*Cobblestone, 400 mm thick*			
B2A-1	A	–	–	CA-1	A	–	–
B2A-2	A	–	–	CA-2	A	–	–
B2A-N-1	A	N	66 × 66 S	CA-M-1	A	M	66 × 66 S
B2A-N-2	A	N	66 × 66 S	CA-M-2	A	M	66 × 66 S
B2A-M-1	A	M	66 × 66 S	CF-1	F	–	–
B2A-M-2	A	M	66 × 66 S	CF-2	F	–	–
B2A-Z-1	A	Z	66 × 66 S	CF-L-1	F	L	66 × 66 S
B2A-Z-2	A	Z	66 × 66 S	CF-L-2	F	L	66 × 66 S
Rubble stone masonry, 400 mm thick				*Rubble stone masonry, 700 mm thick*			
R4D-1	D	–	–	R7E-1	E	–	–
R4D-N-1	D	N	66 × 66 S	R7E-2	E	–	–
R4D-N-2	D	N	66 × 66 S	R7E-M-1	E	M	66 × 66 S
R4D-M-1	D	M	66 × 66 S	R7E-M-2	E	M	66 × 66 D
R4D-M-2	D	M	66 × 66 S	R7E-Z-1	E	Z	66 × 66 S
R4D-Z-1	D	Z	66 × 66 S	R7E-Z-2	E	Z	66 × 66 D
R4D-Z-2	D	Z	66 × 66 S				

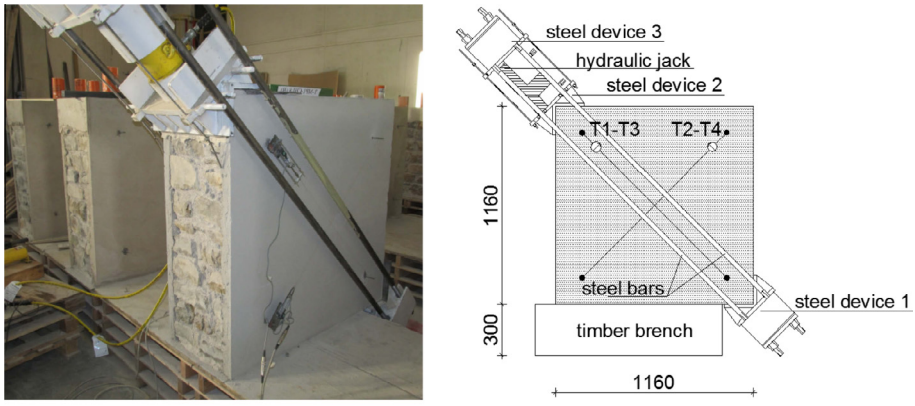

Fig. 2. Picture (a) and drawing (b) of the experimental apparatus for diagonal compression tests mounted on a specimen.

the ductility of the specimens subjected to diagonal compression. The terms $\varepsilon_{c,0.8}$ and $\varepsilon_{t,0.8}$ are compressive and tensile strains, respectively, measured along the diagonals of the specimen in correspondence of a post-peak load 20% lower than the maximum one.

The effectiveness of the strengthening technique is evidenced in Fig. 7, where both the ratios $P_{max(R)}/P_{max(U)}$ (Fig. 7a) and $\mu_{(R)}/\mu_{(U)}$ (Fig. 7b) are reported. The latter represents the ratio between the ductility of RM and URM.

The RM resistance is about 1.78 times that of URM ones for solid brick samples, about 1.87 times in the specimens made with rubble stones, 400 mm thick, whereas about 1.70 times in the rubble stone specimens 700 mm thick. For cobblestone masonry, the resistance of RM was about 3.18 and 4.53 times that of the URM, for type A and type F mortars respectively.

The comparison of the results of specimens with the same thickness (cobblestone and rubble stone masonry 400 mm thick) reinforced with type M mortar, evidences that the resistance increments are greater in weaker masonry, as evidenced also in [33].

The resistance increments of 700 mm thick rubble stone specimens are not significantly affected by the type of GFRP mesh used (S or D type), due to the low influence of the reinforcement before the crack occurrence [33]. GFRP mesh plays an important role after the cracking of mortar coating, contrasting the rapid decrease of resistance in the mortar: a greater amount of reinforcement results, in general, in a higher stiffness of the post-peak branch, as emerged comparing P–ε_c curves of specimens R7E-Z-1 and R7E-Z-2. Instead, a local detachment of the coating in the mesh plane occurred in specimen R7E-M-2, resulting in a larger decrease of resistance.

Experimental results evidence also the essential contribution of the GFRP mesh in the post-peak branch: the composite mesh, in fact, prevents the abrupt decrease of the resistance of solid brick URM (where $\mu_{(U)}$ was, on average 3.3), resulting in a ductility ratio $\mu_{(R)}/\mu_{(U)}$ of about 7.5. This result is very important as it shows how the presence of the mesh reduces significantly the brittle behavior of the URM masonry, avoiding the sudden collapse of the wall after cracking. In stone masonry, because of the interlocking effect, the resistance reduction after cracking of URM is considerably lower than that of solid brick URM: $\mu_{(U)}$ is about 35.2 for cobblestone masonry, 17.4 for rubble stone masonry 400 mm thick and 27.8 for rubble stone masonry 700 mm thick. The GFRP mesh contrasts the crack opening in the coating, allowing to maintain a resistance larger than 80% of the maximum one up to displacement values greater than those of URM specimens: ductility ratios $\mu_{(R)}/\mu_{(U)}$ are on average 1.7 for cobblestone masonry, 2.0 for rubble stone masonry 400 mm thick and 2.4 for rubble stone masonry 700 mm thick. In general, it can be observed that the lower is the ductility of the URM $\mu_{(U)}$, the higher is the ductility ratio $\mu_{(R)}/\mu_{(U)}$.

4. Discussion of the results

The diagonal compression tests permit to assess the principal tensile strength of the specimens. In particular, according to the provision of the standard RILEM TC 76-LUM [45], the principal tensile strength f_t at the center of a square sample subjected to diagonal compression can be calculated with the relationship:

$$f_t = \alpha \frac{P_{max}}{b \cdot t}, \tag{1}$$

where P_{max} is the maximum load reached in the test, b and t are the width and the thickness of the specimen, respectively, and α is a coefficient assumed equal to 0.5. As evidenced in [33], the use of this value for results as the most appropriate to estimate an average equivalent tensile strength of the masonry associated to the maximum load both for URM and RM specimens. It is observed that the value of f_t calculated through Eq.(1) corresponds to the tensile strength of masonry associated to a ratio between the principle stresses σ_I/σ_{III} equal to −3.2 [46,47] and referred to a loading direction angle of 45° with respect to the orientation of the bed joints.

The tensile strengths of URM and RM specimens calculated through Eq. (1) are reported in the third column of Table 6. The tested URM specimens made with solid bricks have an average tensile strength equal to 0.33 MPa, whereas those made with rubble stone provide values equal to 0.26 MPa, for specimens 400 mm thick, and 0.25 MPa for specimens 700 mm thick. Lower values of f_t was obtained for cobblestone URM specimens: 0.13 MPa, for mortar type A, and 0.05 MPa for mortar type F. The tensile resistance of RM was evaluated assuming for t in Eq. (1) the thickness of the unreinforced sample t_m and on average resulted equal to 0.59 MPa, for solid brick samples, 0.49 MPa, for rubble stone specimens 400 mm thick, 0.43 MPa, for rubble stone specimens 700 mm thick, 0.40 MPa, for cobblestones with mortar type A, and 0.24 MPa for cobblestone specimens made with mortar F.

The results of the experimental campaign allowed developing an analytical formulation for the prediction of the resistance to diagonal compression of RM.

Assuming the hypothesis of no-slip between masonry and mortar coating, an estimate of the diagonal compression resistance of the RM specimens was at first conducted by the summation of the average resistance of URM specimens $P_{max(U)}$ and the resistance of the mortar coating P_c. The latter was derived from

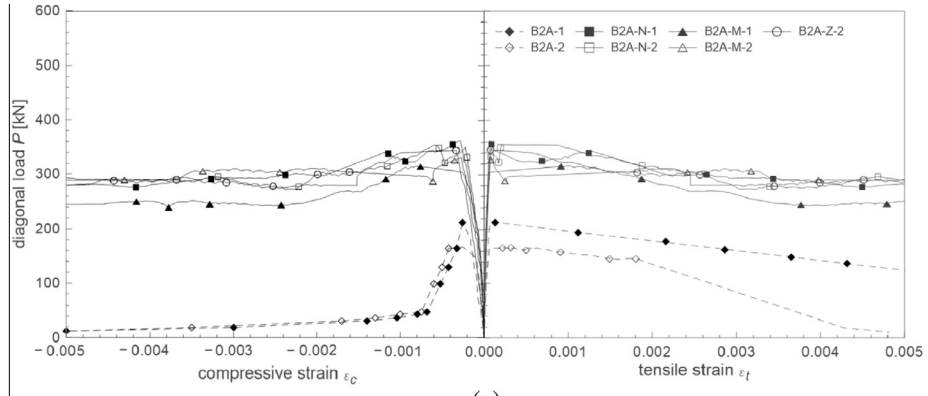

(a)

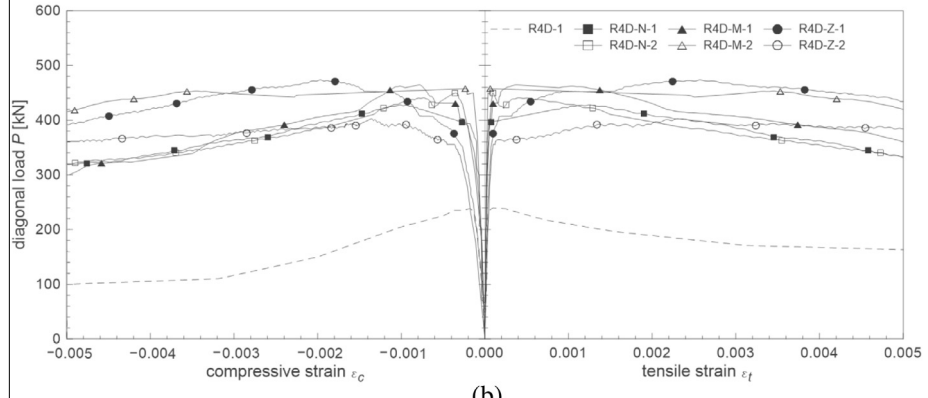

(b)

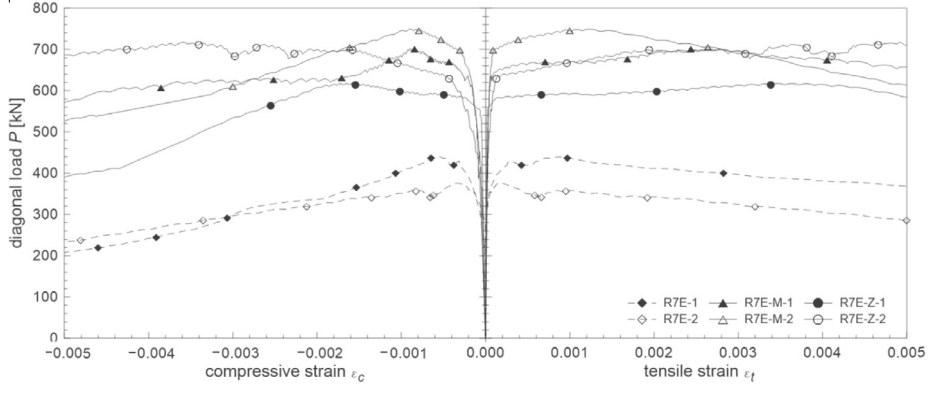

(c)

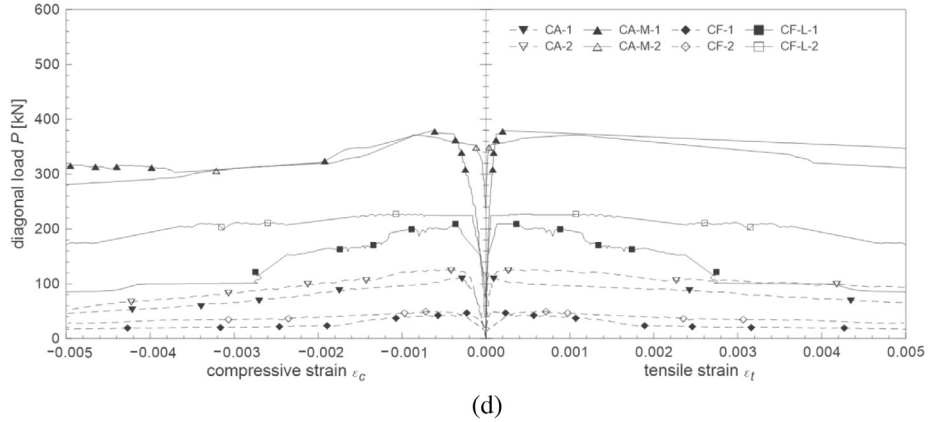

(d)

Fig. 3. Diagonal load P versus compressive strain ε_c curves: solid brick masonry (a) cobblestone masonry (b) and rubble stone masonry 400 mm thick (c) and 700 mm thick (d).

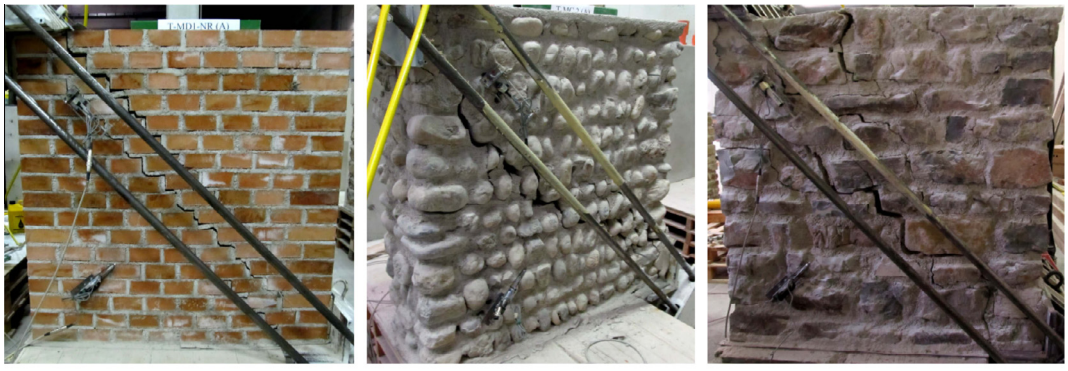

(a) (b) (c)

Fig. 4. Failure mode of URM specimens subjected to diagonal compression tests: solid brick (a), cobblestone (b) and rubble stone (c).

(a) (b) (c)

Fig. 5. RM specimens: cracking configuration of the mortar coating just before reaching the peak resistance (a) and at $\varepsilon_c \cong 1\%$ (b); detail of the GRFP mesh damage state at the end of the test, after removing a portion of mortar coating (c).

Table 5
Test results: maximum diagonal compressive load (P_{max}), ratio between the maximum load of RM and URM specimens ($P_{max(R)}/P_{max(U)}$), yielding (γ_y) and post-peak shear strains ($\gamma_{0.8}$), ductility (μ) and ratio between the ductility of RM and URM ($\mu_{(R)}/\mu_{(U)}$).

Specimen	P_{max} [kN]	$\frac{P_{max(R)}}{P_{max(U)}}$ –	γ_y [‰]	$\gamma_{0.8}$ [‰]	μ –	$\frac{\mu_{(R)}}{\mu_{(U)}}$ –	Specimen	P_{max} [kN]	$\frac{P_{max(R)}}{P_{max(U)}}$ –	γ_y [‰]	$\gamma_{0.8}$ [‰]	μ –	$\frac{\mu_{(R)}}{\mu_{(U)}}$ –
Solid brick masonry, 250 mm thick							*Cobblestone masonry, 400 mm thick*						
B2A-1	214.2	–	0.49	0.65	1.33	–	CA-1	110.4	–	0.12	4.28	36.05	–
B2A-2	169.5	–	0.43	2.29	5.34	–	CA-2	126.0	–	0.11	5.34	47.56	–
B2A-N-1	363.4	1.89	0.30	6.96	22.99	6.89	CA-M-1	379.5	3.21	0.15	8.72	58.01	1.39
B2A-N-2	355.2	1.85	.027	7.22	26.33	7.89	CA-M-2	371.5	3.14	0.11	9.56	85.11	2.04
B2A-M-1	315.9	1.65	0.21	5.08	23.66	7.09	CF-1	46.7	–	0.14	3.39	24.18	–
B2A-M-2	332.4	1.73	0.30	9.68	32.20	9.65	CF-2	49.8	–	0.14	4.52	33.09	–
B2A-Z-1	345.3	1.80	0.39	10.33	26.82	8.04	CF-L-1	209.2	4.34	0.14	4.62	32.11	1.12
							CF-L-2	227.4	4.72	0.15	9.50	65.08	2.27
Rubble stone masonry, 400 mm thick							*Rubble stone masonry, 700 mm thick*						
R4D-1	238.6	–	0.49	2.60	17.37	–	R7E-1	439.5	–	0.23	7.58	32.94	–
R4D-N-1	427.7	1.79	0.43	8.37	34.39	1.98	R7E-2	376.0	–	0.27	6.05	22.61	–
R4D-N-2	449.6	1.88	0.30	6.78	24.14	1.39	R7E-M-1	702.1	1.72	0.19	14.73	79.34	2.86
R4D-M-1	464.6	1.95	0.27	7.80	33.60	1.93	R7E-M-2	749.5	1.84	0.19	8.50	44.12	1.59
R4D-M-2	457.6	1.92	0.21	10.03	42.52	2.45	R7E-Z-1	617.4	1.51	0.17	10.69	63.49	2.29
R4D-Z-1	473.4	1.98	0.30	13.55	29.54	1.70	R7E-Z-2	717.2	1.76	0.22	17.74	78.98	2.84
R4D-Z-2	402.8	1.69	0.39	19.14	41.58	2.39							

the tensile strength of mortar $f_{t,c}$ (Table 2) through Eq. (1) assuming as t the thickness of the two layers of plaster ($2t_c$). Due to the low geometrical percentage ($A/bt_c \sim 0.5\%$) and to the low modular ratio ($E/E_c \sim 2$), the GFRP mesh effect may be assumed negligible up to the crack formation in the mortar coating (A and E are the cross section of mesh wires and the Young modulus of the composite). Comparing these preliminary analytical predictions with the experimental results emerges a quite good assessment of the RM resistance for solid brick masonry and rubble stone masonry (400 mm thick), in case of type M mortar. On the contrary, important overestimates of the resistance were obtained for stronger mortars (type Z) and relevant underestimates for softer ones (type N). The predicted resistance of the 700 mm thick rubble stone RM is good for type Z mortar and underestimated for type M mortar; cobblestone RM resistances are all underestimated.

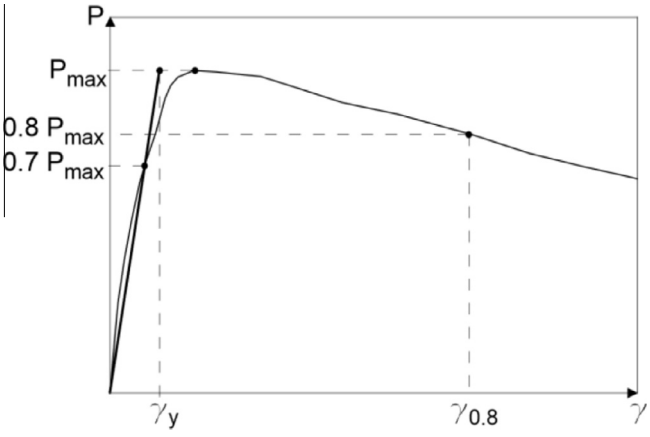

Fig. 6. Individuation on the yield deformation γ_y and of the post-peak shear strain $\gamma_{0.8}$ in P–γ curve.

Then, a modification factor β was defined as the ratio between the experimental resistance of RM wallettes $P_{max(R)}$ and the preliminary analytical prediction ($P_{max(U)} + P_c$):

$$\beta = \frac{P_{max(R)}}{(P_{max(U)} + P_c)} \tag{2}$$

It was noted that for masonry with equal mechanical characteristics and for the range of mortar coating tested, the β coefficient assumed a linear trend in function of the tensile strength of mortar, with values decreasing as the mortar strength increases. The values of the β coefficient in function of the tensile strength of the mortar used for the coating are plotted in Fig. 8. The analytical functions of the best fitting tendency lines are also displayed; no tendency curve is drawn for cobblestone masonry, as the specimens are made with masonry of different mechanical characteristics (see Table 4).

From tendency curves, the values of the modification factor were calculated, for each masonry type, in relation of the mortar coating resistance and the resistance of RM specimens was derived analytically through the relationship:

$$P^*_{max(R)} = \beta^* \cdot (P_{max(U)} + P_c), \tag{3}$$

where the superscript (*) distinguishes the calculated values from the experimental ones.

It is also possible, through Eq. (1), to derive the predicted equivalent principal tensile strengths of RM, $f^*_{t(R)}$, and compare this values with the experimental results, to check the accuracy of the analytical formulation. The analytical calculation of the principal tensile strength $f^*_{t(R)}$ and the comparisons with the experimental results are reported in Table 6 and illustrated in Fig. 9. The evaluations are very good for all specimens considering the scatter of the masonry material: the error percentage $\Delta_{err(ft)}$ ranges between −6.78% and +10.10%, with a coefficient of variation equal to 5.30% points.

The tendency of the modification factor evidenced in the analytical formulation is strictly related to the dissipative capacity of both the RM and the URM. The behavior of the reinforced mortar coating can be obtained subtracting, for each compressive strain value, the ordinates of URM curve to the RM ones.

In Fig. 10, the average P–ε_c curves referred to solid brick masonry are schematized; in particular, Fig. 10a refers to type M mortar coating, Fig. 10b to type Z and Fig 10c to type N. From all the curves emerged that, after the occurrence of the first cracking (P_c), the reinforced mortar coating has a gradual stiffness reduction and a significant resistance increase, due to the presence of the GFRP mesh. In fact, a relevant tension stiffening effect of the plaster among the cracks prevents the abrupt decrease of the resistance. Furthermore, in the cracked areas of the mortar coating, the formation of a strut-and-tie mechanism composed by the tensed GFRP wires and the compressed struts of mortar which oppose to the meshes deformation occurs. Then, after the first cracking, the resistance of the reinforced mortar coating increases up to reaching the spalling of the mortar struts or the wires rupture.

It can be observed that in a masonry with a brittle behavior, such as solid brick, the resistance of the RM specimens $P_{max(R)}$ can be evaluated as the sum of the resistances of the masonry $P_{max(U)}$ and of the plain coating P_c only in case of simultaneous cracking of both components. This type of collapse is evidenced in Fig. 10a, where AD = AC + AB (with AC = $P_{max(U)}$ and AB = P_c) and, thus, $\beta^* \approx 1$. Otherwise, if the cracking occurs first in the masonry, the maximum load of the specimen is reached without exploiting the whole resistance of the plaster, as emerges in Fig. 10b, where AD = AC + AB but AB < EF (= P_c), therefore $\beta^* < 1$. In the two cases of collapse described above, the resistance of the reinforced coating, although higher than that of the plain plaster, does not affect the resistance of RM, as the abrupt decrease of the load in the URM is larger than the load increment in the reinforced coating after the cracking. On the contrary, when the cracking occurs first in the coating, the post cracking resistance of the

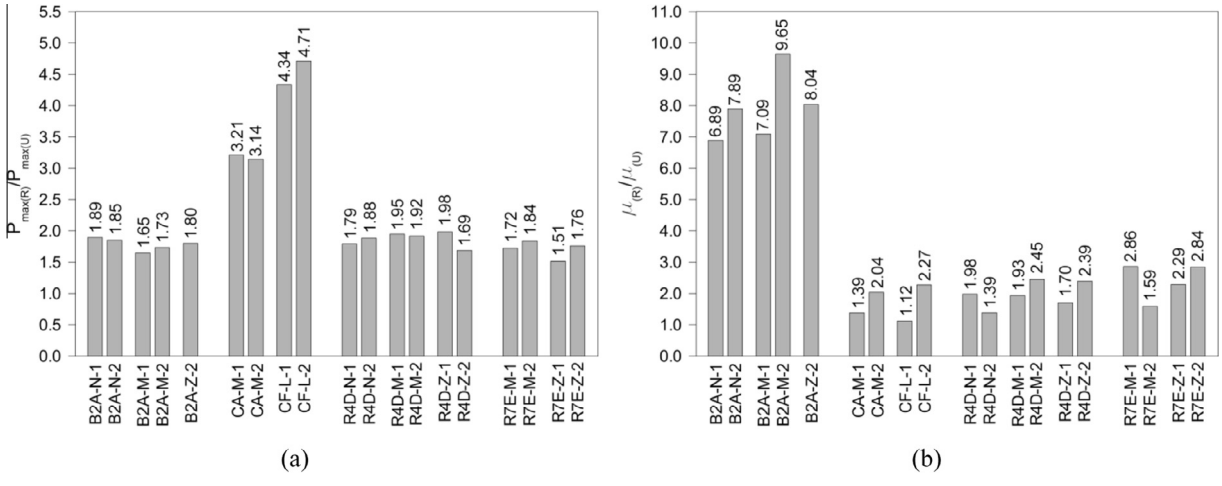

Fig. 7. Effectiveness of the strengthening technique evidenced through ratio between RM and URM specimens in terms of resistance (a) and ductility (b).

Table 6
Maximum diagonal load (P_{max}), principal tensile strength derived from experimental results (f_t), analytical prediction of the principal tensile strength of RM samples (f_t^*) and comparisons with experimental results in terms of error percentage ($\Delta_{err(ft)}$).

Specimen	P_{max} [kN]	f_t [MPa]	$P_{max(U)}$ [kN]	P_c [kN]	$P_{max(U)} + P_c$ [kN]	β –	β^* –	$P^*_{max(R)}$ [kN]	f_t^* [MPa]	$\Delta_{err(ft)}$ %
Solid brick masonry, 250 mm thick										
B2A-1	214.2	0.369	–	–	–	–	–	–	–	–
B2A-2	169.5	0.292	–	–	–	–	–	–	–	–
B2A-N-1	363.4	0.627	191.9	107.2	299.1	1.22	1.16	346.9	0.598	−4.61
B2A-N-2	355.2	0.612	191.9	107.2	299.1	1.19	1.16	346.9	0.598	−2.27
B2A-C-1	315.9	0.545	191.9	146.2	338.0	0.93	1.02	344.8	0.594	9.08
B2A-C-2	332.4	0.573	191.9	146.2	338.0	0.98	1.02	344.8	0.594	3.75
B2A-Z-1	345.3	0.595	191.9	200.5	392.3	0.88	0.83	325.6	0.561	−5.65
Cobblestone, 400 mm thick										
CA-1	110.4	0.119	–	–	–	–	–	–	–	–
CA-2	126.0	0.136	–	–	–	–	–	–	–	–
CA-C-1	379.5	0.409	118.2	146.2	264.4	1.44	1.42	375.45	0.405	−1.08
CA-C-2	371.5	0.400	118.2	146.2	264.4	1.41	1.42	375.45	0.405	1.14
CF-1	46.7	0.050	–	–	–	–	–	–	–	–
CF-2	49.8	0.054	–	–	–	–	–	–	–	–
CF-L-1	209.2	0.225	48.3	76.6	124.9	1.68	1.75	218.51	0.235	4.65
CF-L-2	227.4	0.245	48.3	76.6	124.9	1.82	1.75	218.51	0.235	−3.89
Rubble stone, 400 mm thick										
R4D-1	238.6	0.257	–	–	–	–	–	–	–	–
R4D-N-1	427.7	0.461	238.6	107.2	345.8	1.24	1.29	446.08	0.481	4.27
R4D-N-2	449.6	0.484	238.6	107.2	345.8	1.30	1.29	446.08	0.481	−0.68
R4D-C-1	464.6	0.501	238.6	146.2	384.8	1.21	1.17	450.22	0.485	−3.16
R4D-C-2	457.6	0.493	238.6	146.2	384.8	1.19	1.17	450.22	0.485	−1.59
R4D-Z-1	473.4	0.510	238.6	200.5	439.1	1.08	1.01	443.49	0.478	−6.29
R4D-Z-2	402.8	0.434	238.6	200.5	439.1	0.92	1.01	443.49	0.478	10.10
Rubble stone, 700 mm thick										
R7D-1	439.5	0.271	–	–	–	–	–	–	–	–
R7D-2	376.0	0.232	–	–	–	–	–	–	–	–
R7E-C-1	702.1	0.432	407.8	146.2	554.0	1.27	1.31	725.74	0.447	3.45
R7E-C-2	749.5	0.462	407.8	146.2	554.0	1.35	1.31	725.74	0.447	−3.27
R7E-Z-1	617.4	0.380	407.8	200.5	608.3	1.01	1.10	669.13	0.412	8.43
R7E-Z-2	717.2	0.442	407.8	200.5	608.3	1.18	1.10	669.13	0.412	−6.78

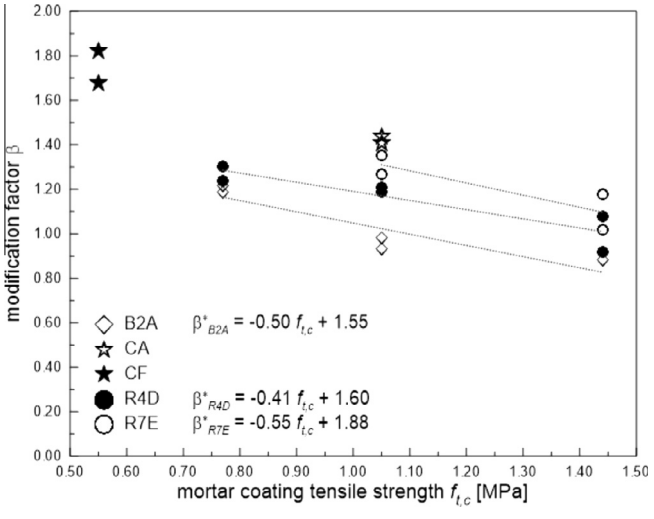

Fig. 8. Trends of the modification factor in function of the tensile strength of the mortar coating.

reinforced mortar coating is partially exploited before the masonry cracking is reached, as shown in Fig. 10c where AD = AC + AB and AB > EF (= P_c), so $\beta^* > 1$.

As evidenced in subsection 3.3, in URM specimens made with stone units a significant interlocking effect caused an attenuated decrease of the resistance after the peak load. These aspect affects the resistance of RM samples, as the gradual decrease of the load in the masonry allows to exploit the whole or part of the post cracking resistance of the reinforced mortar coating, as evidenced in Fig. 11 ($P_{max(R)}$ = AD = AC + AB). In particular Fig. 11a and b schematically represent the behavior of rubble stone specimens 400 mm thick strengthen with a type N and type Z reinforced mortar coating, respectively. In Fig. 11a the RM resistance (AD = AC + AB) is much higher than the summation of $P_{max(U)}$ and P_c (GH + EF), while in Fig. 11b AC + AB ≈ GH + EF. Therefore, in RM specimens where the type N mortar was used, results $\beta^* > 1$ while for specimens reinforced with type Z mortar the modification factor is approximately unitary. The behavior of the

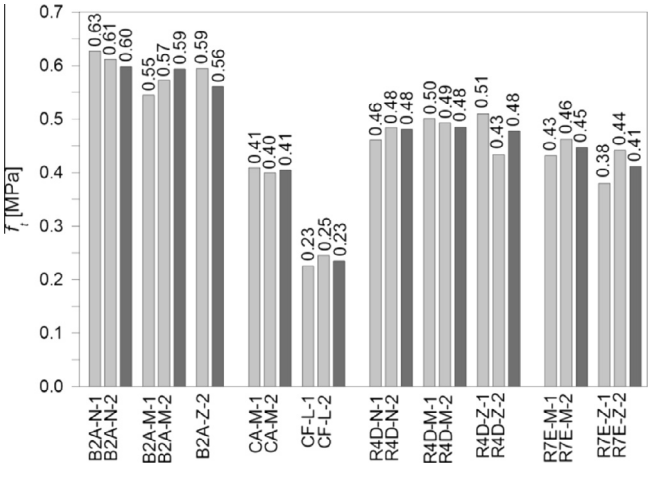

Fig. 9. Comparison between experimental results and analytical predictions (dark gray) of the principal tensile strength of RM specimens.

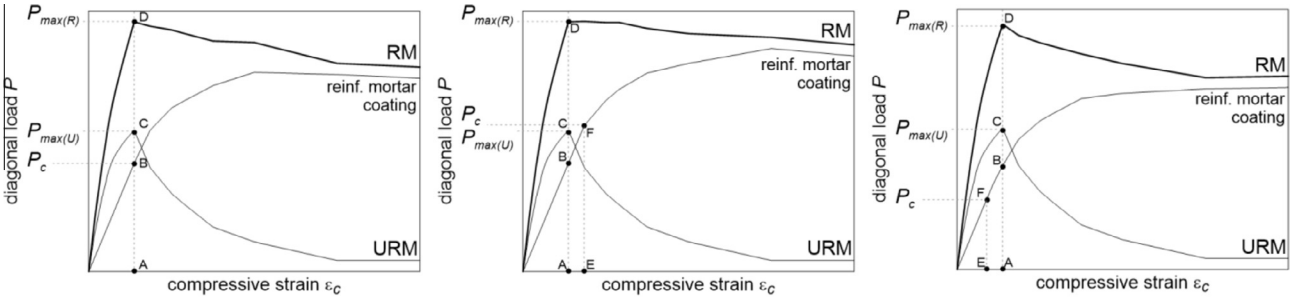

Fig. 10. The three collapse cases in solid brick RM specimens: simultaneous cracking of masonry and reinforced coating (a), cracking occurs first in the masonry (b) and cracking occurs first in the mortar coating (c).

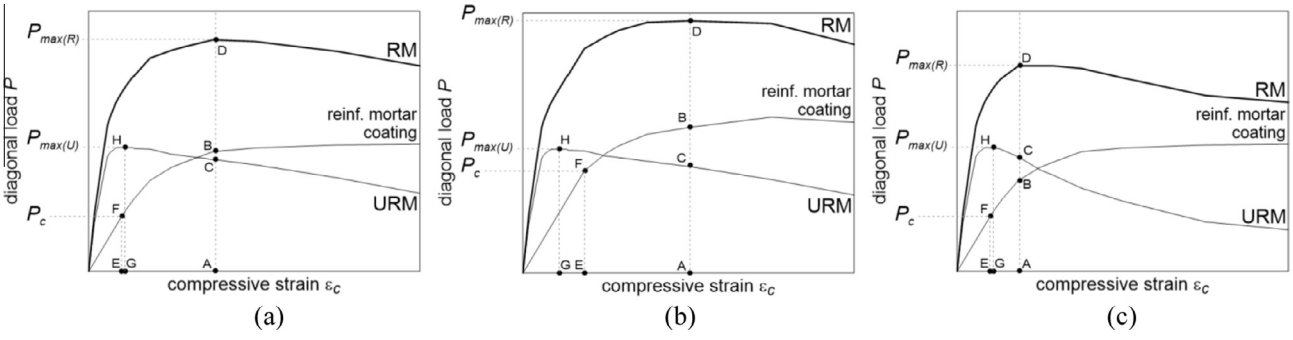

Fig. 11. Possible collapse cases in stone RM specimens.

specimens strengthen with type M mortar and the value of the corresponding modification factor is intermediate between the cases of Fig. 11a and b.

Finally, comparing Fig. 11a–c, it is evidenced that the exploitation of the post cracking resistance of the reinforced mortar coating (AB) is significantly influenced by the softening branch after the maximum resistance of the URM.

In general, the different collapse cases are strictly related to the characteristics of both the masonry and the coating (i.e. post cracking behavior, stiffness, tensile strengths, thicknesses, etc.), thus the values of the coefficient $\beta*$ assumed in the analytical formulation are useful for the type of masonry and of reinforcement analyzed in the paper. The use of similar formulations is obviously allowed also for different materials, but it is necessary to determine the correct value of the modification factor through experimental tests or numerical simulations.

5. Conclusions

The results of several diagonal compression test carried out on masonry specimens are reported in the paper to check the effectiveness of an in-plane strengthening technique based on the application, on both faces of the wall, of a mortar coating reinforced with GFRP meshes. The effectiveness was evaluated through diagonal compression tests considering different mechanical characteristics for the mortar coating. Different types of masonry were considered for the tests: solid brick, cobblestones, and rubble stones.

In URM specimens a diagonal crack occurred along the force direction: in solid brick masonry, the crack spread rapidly, resulting in an abrupt decrease of masonry resistance while in samples made with rubble units or cobblestones a slower decrease of the resistance occurred after crack formation. In RM specimens several parallel cracks progressively formed in the mortar coating, up to the gradual failure of the mesh wires.

The experimental results evidenced that the resistance increment in RM specimens is about 70–90% the resistance of the URM ones for solid brick and rubble stones masonry and about 220% and 350% for cobblestone masonry with type A (stronger) and type F (softer) mortars, respectively. Considerable improvements emerged also in the dissipative capacity of solid brick samples: the ductility of RM was about 8 times that of URM. Lower increments emerged for rubble stone (2–2.4 times URM) and cobblestone (1.7 times URM) RM specimens, as the URM samples show a significant ductile behavior due to the interlocking effect. Furthermore, it was evidenced that the effectiveness of the technique is not appreciably affected by the resistance of the coating. From the results of the experimental tests the equivalent principal tensile strengths of the specimens associated to the peak loads were derived applying the RILEM approach [45].

An analytical formulation was then proposed to assess the resistance and, thus, the tensile strength of RM specimens considering the contribution of the URM and that of the mortar used in the coating. The calculation of the resistance of RM was conducted by adding to the URM resistance that of the coating and multiplying the result by a coefficient calibrated according to the characteristics of the coupled materials. The analytical predictions showed a good reliability and evidenced that the simple summation of the resistances of the masonry and the coating in not always on the safe side. The formulation was calibrated on the basis of the experimental results herein presented; to give general validity some more tests and numerical simulations are in progress. The proceed of the research should investigate in depth the actual stress state of the RM panels, focusing on the interaction between the reinforced layers and the masonry. These information appear useful to elaborate a numerical model reliable to predict the behavior of reinforced masonry, as to

extend the investigation on the strengthening technique effectiveness to a wider range of parameters such as masonry and coating thickness, tensile strength, stiffness.

Acknowledgements

This paper is based on part of the results of a research project financed by the composite engineering factory FibreNet s.r.l., Udine, Italy. The grant of the Italian Civil Protection ReLUIS 2014 is gratefully acknowledged. Moreover, the useful help provided by Mr. Andrea Cernigoi, technician of the Laboratory of Testing Materials, University of Trieste, and of Mr. Allen Dudine during the execution of tests needs to be mentioned.

References

[1] Tomazevic M, Weiss P, Lutman M. Influence of floors and connection of walls on seismic resistance of old brick masonry buildings. Lubiana (SLO): Institute for Testing and Research in Materials and Structures; 1994.
[2] Gattesco N, Macorini L. In-plane stiffening techniques with nail plates or CFRP strips for timber floors in historical masonry buildings. Constr Build Mater 2014;58:64–76.
[3] Tomazevic M, Api V. The strengthening of stone masonry walls by injecting the masonry-friendly grouts. Eur Earthquake Eng 1993;1:10–20.
[4] Binda L, Modena C, Baronio G, Abbaneo S. Repair and investigation techniques for stone masonry walls. Constr Build Mater 1994;11(3):133–42.
[5] Vintzileou E, Miltiadou-Fezans A. Mechanical properties of three-leaf stone masonry grouted with ternary or hydraulic lime-based grouts. Eng Struct 2008;30(8):2265–76.
[6] Tomazevic M, Sheppard P. The strengthening of stone-masonry buildings for revitalizing in seismic regions. In: 7th Eur. conf. on earthq. eng., vol. 5. Athens, GR; 1982. p. 285–82.
[7] Alcocer SM, Ruiz J, Pineda JA, Zepeda, JA. Retrofitting of confined masonry walls with welded wire mesh. In: Proc. 11th World conference on earthquake engineering, vol. 1471. Acapulco, Mexico; 1996.
[8] ElGawady M, Lestuzzi P, Badoux M. A review of conventional seismic retrofitting techniques for URM. In: Proc. 13th international brick and block masonry conference. Amsterdam, Netherlands; 2004.
[9] Valluzzi MR, Binda L, Modena C. Mechanical behaviour of historic masonry structures strengthened by bed joints structural repointing. Constr Build Mater 2005;19(11):63–73.
[10] Ismail N, Petersen RB, Masia MJ, Ingham JM. Diagonal shear behaviour of unreinforced masonry wallets strengthened using twisted steel bars. Constr Build Mater 2011;25(12):4386–93.
[11] Chrysostomou CZ, Demetriou T, Pittas M. Conservation of historical Mediterranean sites by innovative seismic-protection techniques. In: Proc. 3rd world conference on structural control, vol. 2. Como, Italy; 2002. p. 947–54.
[12] Corradi M, Borri A, Vignoli A. Experimental evaluation of the in-plane shear behaviour of masonry walls retrofitted using conventional and innovative methods. J Br Mason Soc 2008;21(1):29–42.
[13] Kadam SB, Singh Y, Li B. Strengthening of unreinforced masonry using welded wire mesh and micro-concrete – behaviour under in-plane action. Constr Build Mater 2014;54:247–57.
[14] Tumialan JG, Huang PC, Nanni A, Silva P. Strengthening of masonry walls by FRP structural repointing. Non-metallic reinforcement for concrete structures. In: 5th International research symposium on fiber reinforced polymer for reinforced concrete structures. Cambridge, UK; 2001.
[15] Turco V, Secondin S, Morbin A, Valluzzi MR, Modena C. Flexural and shear strengthening of un-reinforced masonry with FRP bars. Compos Sci Technol 2006;66(2):289–96.
[16] Petersen R, Masia M, Seracino R. In-plane shear behavior of masonry panels strengthened with NSM CFRP strips. I: experimental investigation. J Compos Constr 2010;14(6):754–63.
[17] Mahmood H, Ingham JM. Diagonal compression testing of FRP retrofitted unreinforced clay brick masonry wallettes. J Compos Constr 2011;15(5):810–20.
[18] Konthesingha KMC, Masia MJ, Petersen RB, Mojsilovic N, Simundic G, Page AW. Static cyclic in-plane shear response of damaged masonry walls retrofitted with NSM FRP strips – an experimental evaluation. Eng Struct 2013;50:126–36.
[19] Triantafillou TC. Strengthening of masonry structures using epoxy-bonded FRP laminates. J Compos Constr ASCE 1998;2(2):96–104.
[20] Valluzzi MR, Tinazzi D, Modena C. Shear behavior of masonry panels strengthened by FRP laminates. Constr Build Mater 2002;16:409–16.
[21] Alcaino P, Santa-Maria H. Shear response of masonry walls with external CFRP reinforcement. In: Proc. of the 14th world conference on earthq. eng. Beijing (CN); 2008.
[22] Mahmood H, Russel AP, Ingham JM. Monotonic testing of unreinforced and FRP-retrofitted masonry walls prone to shear failure in an earthquake. In: Proc. of the 14th world conference on earthq. eng. Beijing (CN); 2008.
[23] Papanicolaou C, Triantafillou T, Lekka M. Externally bonded grids as strengthening and seismic retrofitting materials of masonry panels. Constr Build Mater 2001;25(2):504–14.
[24] Umair SM, Numada M, Meguro K. In plane behavior of polypropylene and frp retrofitted brick masonry wallets under diagonal compression test. In: Proc. of the 15th world conference on earthq. eng. Lisboa (PT); 2012.
[25] Parisi F, Iovinella I, Balsamo A, Augenti N, Prota A. In-plane behaviour of tuff masonry strengthened with inorganic matrix–grid composites. Compos B 2013;45(1):1657–66.
[26] Faella C, Martinelli E, Nigro E, Paciello S. Tuff masonry walls strengthened with a new kind of C-FRP sheet: experimental tests and analysis. In: Proc. of the 13th world conference on earthq. eng. Vancouver (CA); 2004.
[27] D'Ambrisi A, Focacci F, Caporale A. Strengthening of masonry-unreinforced concrete railway bridges with PBO-FRCM materials. Compos Struct 2013;102:193–204.
[28] Carozzi FG, Milani G, Poggi C. Mechanical properties and numerical modelling of fabric reinforced cementitious matrix (FRCM) systems for strengthening of masonry structures. Compos Struct 2014;107:711–25.
[29] Aldea CM, Mobasher B, Jain N. Cement-based matrix–grid system for masonry rehabilitation. ACI Spring Convention 2005:141–56.
[30] Manzoni E, Dusi A, Mezzi M. Polypmeric grid for a cost effective enhancement of the seismic performance of masonry buildings. In: Proc. of the 14th world conference on earthq. eng. Beijing (CN); 2008.
[31] Özkan C, Ökten MS, Gençoğlu M, Güler K. Experimental investigation of infill walls strengthened by cementitious matrix-fabric compsites. In: Proc. of the 15th world conference on earthq. eng. Lisboa (PT); 2012.
[32] D'Ambrisi A, Mezzi M, Caporale A. Experimental investigation on polymeric net-RCM reinforced masonry panels. Compos Struct 2013;105:207–15.
[33] Gattesco N, Boem I, Dudine A. Diagonal compression tests on masonry walls strengthened with a GFRP mesh reinforced mortar coating. Bull Earthquake Eng 2014. http://dx.doi.org/10.1007/s10518-014-9684-z.
[34] Borri A, Castori G, Corradi M, Sisti R. Masonry wall panels with GFRP and steel-cord strengthening subjected to cyclic shear: an experimental study. Constr Build Mater 2014;56:63–73.
[35] Chrysostomou CZ, Asteris PG. On the in-plane properties and capacities of infilled frames. Eng Struct 2012;41:385–402.
[36] Gattesco N, Boem I. Out-of-plane behaviour of masonry walls strengthened with a GFRP reinforced mortar coating. In: Proc. of the 9th int. mason. conf. Guimaraes (PT); 2014.
[37] CEN. UNI-EN 1998-1:2005 – Eurocode 8 – design of structures for earthquake resistance – part 3: assessment and retrofitting of buildings; 2005.
[38] FEMA 274. NEHRP commentary on the guidelines for the seismic rehabilitation of buildings. Washington, DC: Federal Emergency Management Agency; 1997.
[39] FEMA 356. Seismic rehabilitation prestandard. Washington, DC: Federal Emergency Management Agency; 2000.
[40] FEMA 547. Techniques for the seismic rehabilitation of existing buildings. Washington, DC: Federal Emergency Management Agency; 2006.
[41] CNR-DT 203/2006. Istruzioni per la progettazione, l'esecuzione ed il controllo di strutture di calcestruzzo armato con barre di materiale composito fibrorinforzato. Roma: CNR; 2006.
[42] Gattesco N, Boem I, Dudine A. Impiego di reti in GFRP per il rinforzo di murature esistenti. Structural 2013;181(22).
[43] Gattesco N, Amadio C, Barelli S, Bedon C, Rinaldin G, Zorzini F. Analisi ciclica di pareti murarie in pietrame rinforzate mediante intonaco armato con rete in GFRP. In: XV Convegno L'Ingegneria Sismica in Italia, ANIDIS. Padova (I); 2013.
[44] Park R. Bull NZ Natl Soc Earthquake Eng 1989;22(3):155–66.
[45] RILEM TC. 76-LUM. Diagonal tensile strength tests of small wall specimens. In: RILEM recommendations for the testing and use of constructions materials. London, UK: E&EN SPON; 1994. p. 488–9.
[46] Froch M. Recent advances in photoelasticity. Trans ASME 1931;55:135–53.
[47] Yokel FY, Fattal SG. Failure hypothesis for masonry shear walls. J Struct Div ASCE 1976;10(ST3):515–32.